Sensors & Transducers, Vol. 182, Issue 11, November 2014, pp. 187-193

Sensors & Transducers

http://www.sensorsportal.com

A Novel 3-DOF Translational Micromanipulation Parallel Manipulator for Vibration Control of Crystal Oscillators

Ze Zhao, Yuanying Qiu, Xuechao Duan
Key Laboratory of Electronic Equipment Structure Design,
Ministry of Education, Xidian University Xi'an, 710071, China
Tel.: +86-029-88203040, fax: +86-029-88203040
E-mail: xazhaoze@sina.com, yyqiu@mail.xidian.edu.cn, xchduan@xidian.edu.cn

Received: 25 July 2014 /Accepted: 30 October 2014 /Published: 30 November 2014

Abstract: This paper presents a novel 3-DOF translational micromanipulating parallel manipulator with single type of linear driving and six passive joints. It is chiefly characterized by the constant Jacobian matrix between the input and output. It also has straightforward inverse and forward kinematics, which facilitate the implementation of real-time control. Aiming at the vibration control purpose for a crystal oscillator in electronic equipments, the compactness of the manipulator is also considered and accomplished in the dimension of 75 mm × 67 mm × 25 mm. We finally achieved the 50 Hz 3DOF translational motions within ± 2 mm × ± 2 mm × ± 2 mm and validated the design with computational simulation. *Copyright © 2014 IFSA Publishing, S. L.*

Keywords: 3-DOF translational motion parallel manipulator, Configuration, Jacobian.

1. Introduction

The crystal oscillator provides precise clock signals for digital microchips such as CPU in modern electronic equipments. For mobile applications, vibrations of the base the crystal oscillator mounted on will lead to the aberrance in output of the crystal oscillator, which inevitably bring about timing disturbance of the microchips [1]. It is consequently desired to achieve the vibration control of crystal oscillator by using a mechanical device with small dimension, high stiffness and high accuracy.

The serial manipulator is not eligible for active vibration control due to the positioning error accumulation of each joint and the poor stiffness [2]. On the contrary, parallel manipulators have several limbs actuated in parallel thus lead to the high accuracy, strong stiffness, favorable mobility and light weight. These facts make them good candidates for micromanipulation applications.

There exist parallel manipulators of many kinds having three translational degrees of freedom, among which the most well-known one is the Delta parallel manipulator by Calvel [3]. And there also are 3-UPU, 3-5R, 3-RPC, 3-PUU and three-dimensional spherical platform manipulator types [4]. However, these manipulators usually have complicated limbs. Taking Delta manipulator for example, it uses 17 links and 21 joints in total. Similarly, the precision micromanipulation robot proposed in [5] has 12 joints. For the application of this paper, it is quite challenging to adopt any configuration mentioned above. Because the micromanipulation of links and joints are still open problems in the manufacturing field. Many researchers used compliant joints instead of traditional rigid joints to overcome the dimension limitation and achieve the micromanipulation of

manipulators [6-9]. However, compared with traditional joints, compliant joints need more driving force and yield less displacement most in the grade of micron. Another consideration lies in that the real action position is not deterministic so that the linear actuation may bring about the nonlinear displacement. Thus the kinematic and dynamical expressions of a compliant mechanism are very complicated and they are difficult to control. Besides, the mechanism performances are not so stable as a result of compliant parts, the performances differ a lot even though they are manufactured in an identical production line and under the same condition [10, 11].

The active/passive double level serial vibration damping solution is proposed in this paper. In this solution, the flexible spring is connected to the base of the vibration at one end, and is connected to the active vibration control mechanism at the other end. This special configuration will effectively reduce the low frequency and large amplitude vibrations. The active vibration damping mechanism will move in antiphase with the vibrations in order to reduce the high frequency and small amplitude vibrations. By integrating the advantages of double level active and passive vibration damping mechanisms, the synthesis vibration control performance of the crystal oscillator is achieved. Within the dimension of ± 2 mm $\times \pm 2$ mm $\times \pm 2$ mm, the vibration damping system manages to the three translational micromanipulation at the frequency of 50 Hz.

2. Structure Design of the Novel Three Translational (3T) Parallel Manipulator

This novel 3T parallel manipulator consists of one mobile platform, three unit heads, one base platform, three actuation motor and three tension springs et al as shown in Fig. 1. The mobile platform is an inverted three pyramid with a regular triangle bottom. The base is a hexagonal board on which the actuation motors are mounted. It also guides the translational movement of the three unit heads connected to the actuator. The unit head has the prism-like shape. The three evenly distributed guide lug boss cooperate with the three notch grooves carved on the unit head of the motors as three translational joints. The oblique planes of the unit head and the oblique planes of mobile platform constitute three planar joints. In order to make the two corresponding oblique planes of the unit head and mobile platform touch each other tightly, the unit head is apt to "pull" the mobile platform. Consequently, these three springs connect the mobile platform to the base in this design, which makes it possible for this 3-DOF manipulator to work smoothly even though this system is put upside down.

The three evenly distributed oblique planes of the unit head compose a pyramid (as shown in Fig. 2 (a), Fig. 2(b)). The three oblique planes of the mobile platform are located in the pyramid consisting of unit head (as shown in Fig. 2 (c), Fig. 2 (d)). When they are in operation, the three oblique planes of unit head constitute a pyramid with fixed slope angles and variant volume and position. Among which the mobile platform translates in three orthogonal directions. The volume of pyramid formed by the three oblique planes determines the *z* value of the mobile platform, while the position of the pyramid determines the planar coordinate of the mobile platform.

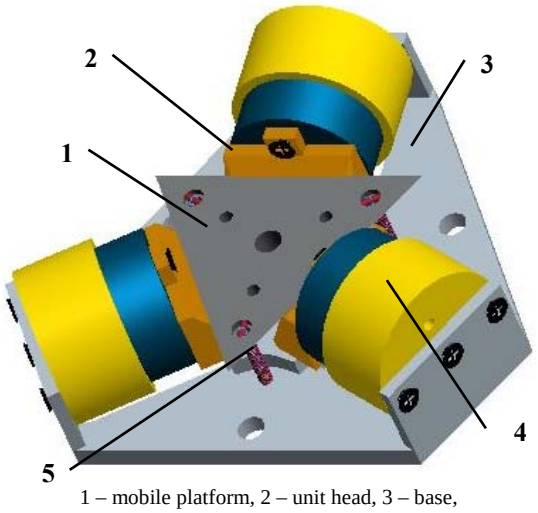

1 – mobile platform, 2 – unit head, 3 – base,
4 – voice coil motor, 5 – tension spring

Fig. 1. Spatial 3T micromanipulation manipulator.

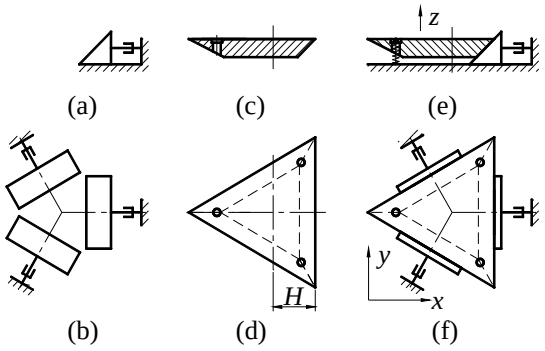

Fig. 2. Schematic of structure.

3. Kinematics

3.1. Inverse Kinematics

The origin of the mobile frame $O_PX_PY_PZ_P$ is located at the center of the top plane of mobile platform. The *XY* plane of the fixed frame *OXYZ* is parallel to the base plane but the origin is located above the base plane with half height of these oblique planes of the unit heads, as shown in Fig. 3.

The position vector $P_i(x_{Pi}, y_{Pi}, z_{Pi})$ denotes the *i*th center of the three centers of the oblique planes of the unit head and can be described in the mobile frame $O_PX_PY_PZ_P$ as follow:

$$\begin{aligned} x_{Pi} &= h_i c\beta_i - C_i s\beta_i \\ y_{Pi} &= h_i s\beta_i + C_i c\beta_i \\ z_{Pi} &= -(H - h_i)/t\alpha \end{aligned}, \quad (1)$$

where *s*, *c* and *t* indicate *sin*, *cos* and *tan* for short, respectively. β_i is the include angle between the center of the *i*th oblique plane and the *x* axis. h_1 is the position of center of oblique plane of the *i*th unit head in X_p. C_1 is the position of center of oblique plane of the *i*th unit head in Y_p. h_2, C_2, h_3 and C_3 indicate the position of unit head II and III. α is the included angle of the vertical direction and the oblique plane of the mobile platform. *H* is the distance between the shape center and the bottom line of the top triangular plane of the mobile platform (Fig. 2(d)), *i*=1, 2, 3.

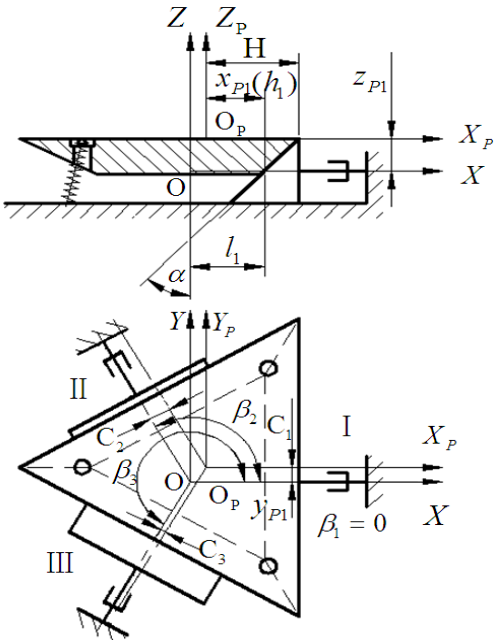

Fig. 3. Frame setup.

The position vector $P = (x, y, z)^{\mathrm{T}}$ represents the position vector of center of the mobile platform *P* in *OXYZ*. The rotation matrix is a unity matrix due to the translational movement of the mobile platform. The position vector of P_i on mobile platform in *OXYZ* can be expressed with $B_i(x_i, y_i, z_i)$:

$$B_i = P_i + P \quad (2)$$

In the fixed frame, l_i is the actuation radius of the *i*th center of oblique plane of unit head. The kinematic constraints are as follow:

$$\begin{aligned} x_i &= l_i c\beta_i \\ y_i &= l_i s\beta_i \\ z_i &= 0 \end{aligned} \quad (3)$$

The displacement equations thus are derived as follow:

$$\begin{aligned} h_i c\beta_i - C_i s\beta_i + x &= l_i c\beta_i \\ h_i s\beta_i + C_i c\beta_i + y &= l_i s\beta_i \\ -(H - h_i)/t\alpha + z &= 0 \end{aligned} \quad (4)$$

By rearranging, the matrix form of inverse kinematic solution of the mobile platform has the following expression:

$$L = J^{-1}P + A, \quad (5)$$

where $J^{-1} = \begin{bmatrix} c\beta_1 & s\beta_1 & -t\alpha \\ c\beta_2 & s\beta_2 & -t\alpha \\ c\beta_3 & s\beta_3 & -t\alpha \end{bmatrix}$, $L = (l_1 \quad l_2 \quad l_3)^T$, $A = H(1 \quad 1 \quad 1)^T$

Further, the inverse solution of velocity and acceleration can also be worked out:

$$\dot{L} = J^{-1}\dot{P}, \quad (6)$$

$$\ddot{L} = J^{-1}\ddot{P}, \quad (7)$$

where $\dot{L} = (\dot{l}_1 \quad \dot{l}_1 \quad \dot{l}_1)^T$, $\dot{P} = (\dot{x} \quad \dot{y} \quad \dot{z})^T$, $\ddot{L} = (\ddot{l}_1 \quad \ddot{l}_2 \quad \ddot{l}_3)^T$, $\ddot{P} = (\ddot{x} \quad \ddot{y} \quad \ddot{z})^T$

3.2. Forward Kinematics

Due to the constant mapping relations between the input and output displacements, and the same case for velocity and acceleration, the forward kinematics of the mobile platform can be derived straightforwardly. By transforming Eq.(5), the forward kinematic solution of the mobile platform can be obtained in matrix form as follow:

$$P = JL + D, \quad (8)$$

where

$$J = \frac{1}{S}\begin{bmatrix} s\beta_2 - s\beta_3 & s\beta_3 - s\beta_1 & s\beta_1 - s\beta_2 \\ c\beta_3 - c\beta_2 & c\beta_1 - c\beta_3 & c\beta_2 - c\beta_1 \\ s(\beta_2 - \beta_3)/t\alpha & s(\beta_3 - \beta_1)/t\alpha & s(\beta_1 - \beta_2)/t\alpha \end{bmatrix},$$

$$D = \begin{bmatrix} 0 \\ 0 \\ H/t\alpha \end{bmatrix},$$

$$S = c\beta_1(s\beta_2 - s\beta_3) + c\beta_2(s\beta_3 - s\beta_1) + c\beta_3(s\beta_1 - s\beta_2)$$

Further, the velocity and acceleration of the mobile platform can be derived as follow:

$$\dot{P} = J\dot{L} \tag{9}$$

$$\ddot{P} = J\ddot{L} \tag{10}$$

The Jacobian matrix of this parallel manipulator is constant, and only depends on the structure of the manipulator but is independent of position of the mobile platform. This is a characteristic of this novel design, which makes it more efficient to conduct the kinematic computation and motion planning. This fact also makes this parallel manipulator eligible for realtime control in active vibration damping application.

4. Dynamics

4.1. Dynamical Equation

This parallel manipulator falls into the multiple rigid body system, the Lagrangian equations are employed to derive the dynamical equations:

$$\frac{d}{dt}\frac{\partial La}{\partial \dot{l}_i} - \frac{\partial La}{\partial l_i} = f_i, \quad i = 1,2,3 \tag{11}$$

where $La=T-U$, La is the Lagrangian function of the system, T and U are kinetic and potential energy functions of the system respectively. l_i is the generalized coordinate pointing to the origin of the fixed frame from the center of oblique place of the unit head. f_i is the generalized external force including the thrust force supplied by the unit heads.

m_i and M denote the mass of the ith unit head and mobile platform, respectively. $\dot{L}$ and $\dot{P}$ denote the velocity of unit heads and mobile platform, respectively. The kinetic energy of the system can be calculated according to their translational movement form as follows:

$$T = \frac{1}{2}\sum_{i=1}^{3} m_i \dot{l}_i^2 + \frac{1}{2}M(\dot{x}^2 + \dot{y}^2 + \dot{z}^2) \tag{12}$$

The mobile platform also bears tensions from the three springs besides gravity. Since the small range of the micromanipulation, we assume that the tension components in X and Y are very small and can be neglected. So only the tension component in Z axis is considered. The XY plane is taken as the zero potential energy planes, and then the potential energy U of the system is:

$$U = Mgz + 3k(z + z_0)^2/2, \tag{13}$$

where Mgz is the gravitational potential energy. $3k(z+z_0)^2/2$ denotes the elastic potential energy of the three spring series. k is the identical stiffness coefficient for the three spring series. z_0 represents the spring elongation when the system locates the zero potential energy plane, which is also stated as preloaded length.

From Eqs. (9), (12) and (13), the Lagrangian function La can be obtained as follows:

$$\begin{aligned} La = T - U = {} & \frac{1}{2}\sum_{i=1}^{3} m_i \dot{l}_i^2 + \\ & \frac{M}{2S^2}\left[(s\beta_2 - s\beta_3)\dot{l}_1^2 + (s\beta_3 - s\beta_1)\dot{l}_2^2 + (s\beta_1 - s\beta_2)\dot{l}_3^2\right]^2 + \\ & \frac{M}{2S^2}\left[(c\beta_3 - c\beta_2)\dot{l}_1^2 + (c\beta_1 - c\beta_3)\dot{l}_2^2 + (c\beta_2 - c\beta_1)\dot{l}_3^2\right]^2 + \\ & \frac{M}{2S^2t^2\alpha}\left[s(\beta_2 - \beta_3)\dot{l}_1^2 + s(\beta_3 - \beta_1)\dot{l}_2^2 + s(\beta_1 - \beta_2)\dot{l}_3^2\right]^2 - \\ & Mg\left[\frac{s(\beta_2 - \beta_3)l_1 + s(\beta_3 - \beta_1)l_2 + s(\beta_1 - \beta_2)l_3}{St\alpha} + H/t\alpha\right] - \\ & \frac{3}{2}k\left[\frac{s(\beta_2 - \beta_3)l_1 + s(\beta_3 - \beta_1)l_2 + s(\beta_1 - \beta_2)l_3}{St\alpha} + H/t\alpha + z_0\right]^2 \end{aligned} \tag{14}$$

Therefore, the dynamical equations of the system are:

$$\begin{aligned} f_1 &= \left\{m_1 + \frac{M}{S^2}\left[\begin{matrix}(s\beta_2 - s\beta_3)^2 + (c\beta_3 - c\beta_2)^2 \\ + s^2(\beta_2 - \beta_3)/t\alpha\end{matrix}\right]\right\}\ddot{l}_1 - G\frac{s(\beta_2 - \beta_3)}{St\alpha} \\ f_2 &= \left\{m_2 + \frac{M}{S^2}\left[\begin{matrix}(s\beta_3 - s\beta_1)^2 + (c\beta_1 - c\beta_3)^2 \\ + s^2(\beta_3 - \beta_1)/t\alpha\end{matrix}\right]\right\}\ddot{l}_2 - G\frac{s(\beta_3 - \beta_1)}{St\alpha} \\ f_3 &= \left\{m_3 + \frac{M}{S^2}\left[\begin{matrix}(s\beta_1 - s\beta_2)^2 + (c\beta_2 - c\beta_1)^2 \\ + s^2(\beta_1 - \beta_2)/t\alpha\end{matrix}\right]\right\}\ddot{l}_3 - G\frac{s(\beta_1 - \beta_2)}{St\alpha} \end{aligned} \tag{15}$$

where $\ddot{l}_i = \ddot{x}c\beta_i + \ddot{y}s\beta_i - \ddot{z}t\alpha$,

$$G = Mg + 3k\left[\begin{matrix}\frac{s(\beta_2 - \beta_3)l_1 + s(\beta_3 - \beta_1)l_2 + s(\beta_1 - \beta_2)l_3}{St\alpha} \\ + H/t\alpha + z_0\end{matrix}\right]$$

4.2. System Power

From Eqs.(9) and (15), the instant powers P_1, P_2 and P_3 of the system can be derived as follows:

$$P_i = f_i \cdot \dot{l}_i \tag{16}$$

4.3. Dynamics Simulation

4.3.1. Case Study of the Dynamics Simulation

As shown in Fig. 4(a), let the mobile platform move along a counter clockwise cylinder screw curve with the start point at (R,0,0) (both the radius of the cylinder and the pitch of the screw are R). In fact the trajectory equation can be formulated as:

$$\begin{aligned} x &= R\cos\theta \\ y &= R\sin\theta \\ z &= R\theta/360^\circ \end{aligned}, \tag{17}$$

where θ is the central angle of the center of the mobile platform during the screw movement and determined by the following expression:

$$\theta = \begin{cases} \frac{1}{2}\varepsilon t^2 & 0 \le t < t_1 \\ \frac{1}{2}\varepsilon t_1^2 + \varepsilon t_1 (t - t_1) & t_1 \le t < t_2 \\ \frac{1}{2}\varepsilon t_1^2 + \varepsilon t_1 (t_2 - t_1) + \frac{1}{2}[2\varepsilon t_1 - \varepsilon (t - t_2)](t - t_2) & t_2 \le t < t_3 \end{cases} \quad (18)$$

The trajectory is planned to be trapezoidal and its acceleration, constant velocity and deceleration periods are shown in Fig. 4(b), Fig. 4(c) and Fig. 4(d), respectively.

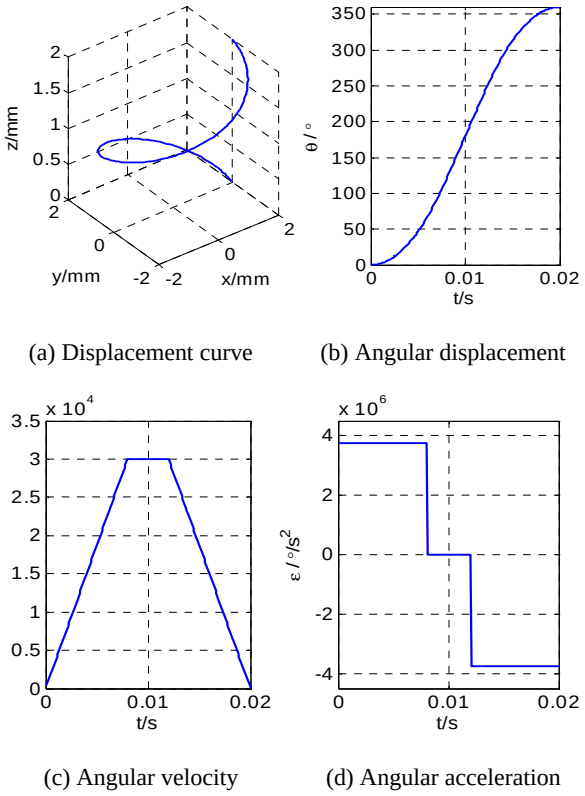

(a) Displacement curve (b) Angular displacement

(c) Angular velocity (d) Angular acceleration

Fig. 4. Motion planning of the mobile platform.

where ε is the angular acceleration, t_1 ,t_2 and t_3 are the transition time point of the motion acceleration. Each of the three sections has the same angular displacement of 120°, the period time is 0.02 s (Depending on the frequency specification of 50 Hz in this vibration damping application). Other parameters used in this simulation are listed in Table 1.

The stiffness coefficient of the three springs is k=50 N/m and preloaded force is 4 N. We can notice in Fig. 5 that the driving force varies between 0 N and 8 N. The actuating speed falls into the range between -1.5 m/s and 1 m/s. The power of driving system is no more than 7 W. This agrees with the hardware specification for this parallel manipulator. Besides, the driving force, velocity and power of the three actuators do not appear identically and periodically with constant phase difference. This phenomenon can be explained by the asymmetrical distribution of the motion trajectory for the three unit head.

Table 1. Parameters in dynamics simulation.

Parameters of the structure				
α(deg)	**β_i(deg)**	*H*(*mm*)	*M*(*g*)	m_i(*g*)
45	0,120,240	12	7	2
Parameters of trajectory				
R (*mm*)		*T*(*S*)		
2		0.02(50 Hz)		

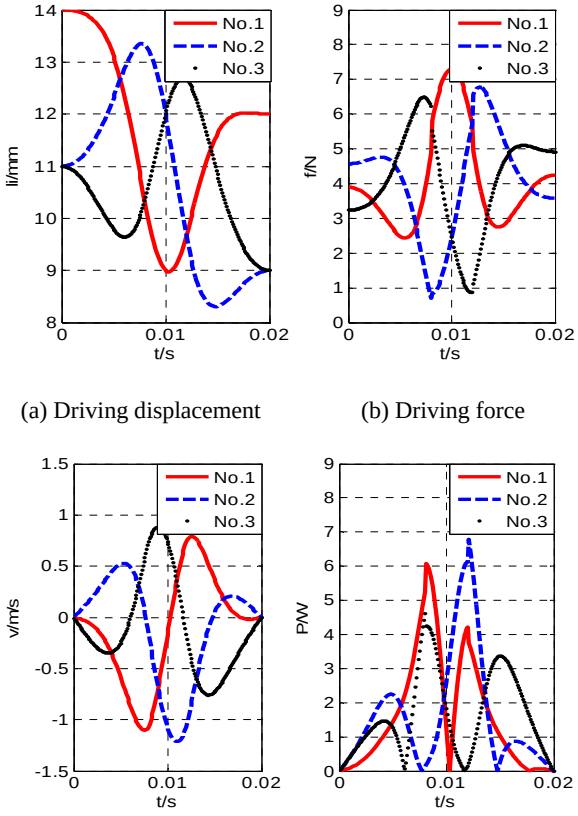

(a) Driving displacement (b) Driving force

(c) Driving velocity (d) Driving power

Fig. 5. Performances of the system in the dynamics simulation.

4.3.2. The Effect of the Variation of Dynamical Factors on the Dynamical Performances

In order to investigate the effect of the variation of dynamical factors on the dynamical performances, large amount of numerical simulation were conducted. From which we draw the conclusion that the driving force and peak power are linearly dependent of the mass of the mobile platform as

shown in Fig. 6(a) and Fig. 6(b), which agrees with our intuition. The driving force is in proportion to the radius of the curve as shown in Fig. 6(c). The driving power is approximately in proportion to the squared radius of the curve as shown in Fig. 6(d). This fact indicates that the radius of the trajectory has great effect on the driving force and power of the system.

As for the period of the trajectory we observed the following result. Decreasing of period of the trajectory will increase the speed of the mobile platform (higher frequency), thus the driving force and power will dramatically increase as shown in Fig. 6(e) and Fig. 6(f). The period plays the role of most importance in the effect of driving force and power.

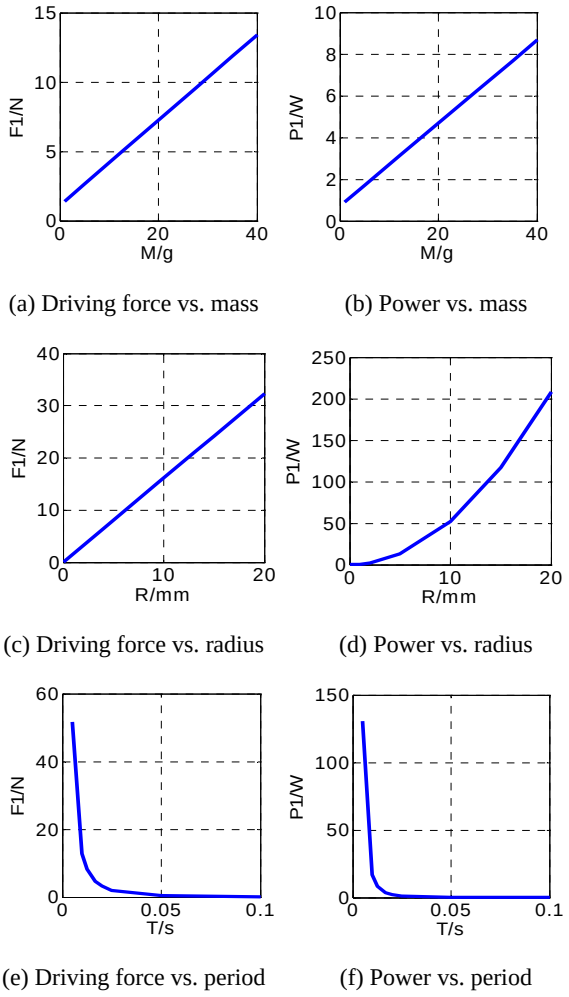

(a) Driving force vs. mass (b) Power vs. mass

(c) Driving force vs. radius (d) Power vs. radius

(e) Driving force vs. period (f) Power vs. period

Fig. 6. Dependence of driving force and power on the main factors.

5. Conclusions

To sum up, the conclusions of this paper can be list as follows:

1) The novel design of a 3-DOF translational parallel manipulator with six joints is proposed in this paper. The mapping relation of displacement, velocity and acceleration merely depends on the structure parameters of the manipulator; and it is independent of position of the end-effector. This constant Jacobian matrix makes it has straightforward kinematics and potential realtime control.

2) This parallel manipulator has a compact dimension of 75 mm × 67 mm × 25 mm. At the same time it is able to supply 3-DOF translational motion within ± 2 mm × ± 2 mm × ± 2 mm at 50 Hz. Numerical simulations show that this manipulator achieves the specification on workspace, rapidity and motion period needed in the serial active and passive vibration damping application.

3) Under the specific motion conditions, the effect of mass of mobile platform, radius of the curve and motion period on the peak driving force and driving power is quantitatively investigated.

Acknowledgements

The authors gratefully acknowledge the financial support of National Natural Science Foundation of China under Grant No. 51175397.

References

[1]. T. Qian, J. Longzhe, et al, Acceleration effect and sensitivity measurement of the quartz, *Journal of Test and Measurement Technology*, Vol. 26, No. 3, 2012, pp. 200-206.

[2]. L. Xinjun, W. Jinsong, et al, Design of 6-DOF parallel microrobotics mechanism, *Journal of Tsinghua University (Science & Technology)*, Vol. 41, No. 8, 2001, pp. 16-20.

[3]. R. Clavel, Delta a fast robot with parallel geometry, in *Proceedings of the International Symposium on Industrial Robot (ISIR)*, Lausanne, Switzerland, 26-28 April 1988, pp. 91-100.

[4]. J. Zhenlin, Y. Yueqing, On the position and workspace of a novel 3-DOF translational spherical platform manipulator, *Chinese Journal of Mechanical Engineering*, Vol. 17, No. 6, 2006, pp. 574-577.

[5]. Zhen Huang, Tieshi Zhao, Fine vernier parallel 3D travel mechanism including screw pair, *China Patent*, 2004, CN200310104278.

[6]. G. Xu, C. Sun, Dynamic modeling and stiffness coefficient analysis of a 3-DOF flexible joint space manipulator, in *Proceedings of the 5th International Conference on Intelligent Human-Machine Systems and Cybernetics (IHMSC)*, 2013, Vol. 2, pp. 171-174.

[7]. X. Shunli, L. Yangmin, Development of a large working range flexure-based 3-DOF micro-parallel manipulator driven by electromagnetic actuators, in *Proceedings of the IEEE International Conference on Robotics and Automation (ICRA)*, 6-10, May, 2013, pp. 4506-4511.

[8]. U. Bhagat, B. Shirinzadeh, Design and analysis of a novel flexure-based 3-DOF mechanism, *Mechanism and Machine Theory*, Vol. 74, April 2014, pp. 173-187.

[9]. L. Yangmin, et al, Design and optimization of an XYZ parallel micromanipulator with flexure hinges,

Journal of Intelligent and Robotic Systems, Vol. 55, No. 4-5, 2009, pp. 377-402.

[10]. F. M. Morsch, J. L. Herder, Design of a generic zero stiffness compliant joint, in *Proceedings of the ASME Design Engineering Technical Conferences & Computers and Information in Engineering Conference*, Montreal, Canada, 15–18 August 2010, DETC2010-28351, 2010.

[11]. Y. Qizhi, et al, Application of the fully compliant mechanism in the parallel micro-motion robots, *Machine Design and Research*, Vol. 21, No. 5, 2005, pp. 45-48.
